Electronic Supplementary Material (ESI) for Journal of Materials Chemistry A.

Supporting information

Cu-doped PtBi Intermetallic Nanofiber Bundles Enhance Alcohol Oxidation Electrocatalysis with Highly CO Tolerance

Jingxian Zhang, Menglei Yuan, Tongkun Zhao, Wenbo Wang, Haoyang Huang, Kairui Cui, Zhanjun Liu, Shuwei Li, Zehui Li*, and Guangjin Zhang*

*Corresponding authors: Z. Li (zehuili@pku.edu.cn) and G. Zhang (zhanggj@ipe.ac.cn)

Experimental sections

Synthesis of Cu-PtBi NFBs

Typically, copper nitrate trihydrate ($Cu(NO_3)_2 \cdot 3H_2O$, 99%, 12.1 mg), bismuth chloride ($BiCl_3$, AR, 15.8 mg), chloroplatinic acid hexahydrate ($H_2PtCl_6 \cdot 6H_2O$, AR, Pt ≥ 37.5%, 0.5 mL, 200 mM), and potassium hydroxide (KOH, 95%, 1.5 g) were firstly added into a solution containing 15 mL of N, N-dimethylformamide (DMF, 95%) and 5 mL of ethylene glycol (EG, 99.5%), followed by ultrasonication for 2 h to form a transparent solution. After that, the mixture was transferred into a 25 mL of Teflon-lined autoclave and heated up to 180 °C for 12 h. The resulting product was centrifuged at 10000 rpm, and then washed three times with an ethanol/ultrapure water (1/1) mixture. Finally, 8 mL of ultrapure water was used to redisperse the resultant Cu-PtBi NFBs materials.

Synthesis of bimetallic PtBi and PtCu NFBs

Except for the lack of $Cu(NO_3)_2 \cdot 3H_2O$ and $BiCl_3$, respectively, similar synthetic procedures were carried out to obtained the PtBi and PtCu NFBs materials.

Materials characterization

Powder X-ray diffraction (PXRD) patterns were collected on a X'PERT PRO MPD diffractometer using Cu Kα radiation (λ = 0.15406 nm) with a scanning range of 5-90 degrees. Transmission electron microscopy (TEM) and high-resolution TEM (HRTEM) images were acquired with a JEM-F200 (Cyro) microscope. High-angle annular dark-field scanning TEM (HAADF-STEM) images, selected area electron diffraction (SAED) patterns, and energy-dispersive spectrometer (EDS) elemental mapping were recorded by a FEI Talos microscope at a working voltage of 200 kV. EDS spectrograms were obtained by scanning electron microscopy (SEM, JSM-7800 (Prime)) with an EDS (X-MaxN50 Aztec). X-ray photoelectron spectroscopy (XPS) experiments were carried out using an ESCALAB 250Xi spectrometer with Al Kα cathode source of 75-150 W under an ultrahigh vacuum. The element contents were determined by the inductively coupled plasma-atomic emission spectrometer (ICP-AES, Agilent 5800VDV).

X-ray absorption fine structure (XAFS) measurements were conducted at the 1W1B-XAFS experimental station of the Institute of High Energy Physics, Chinese Academy of Sciences (Beijing). The signals were collected under transmission mode with the energy calibrated by using commercial

Pt/C. All the XAFS sample powders were pressed and glued to 3M tape for the analyses at the Pt L_3-edge. X-ray absorption near edge structure (XANES) and extended X-ray absorption fine structure (EXAFS) data were processed via the Athena and Artemis programs from the IFEFFIT XAFS analysis software[1].

Estimation of strain from PXRD and EXAFS.

The strain of Cu-PtBi NFBs, *s*, was obtained by the following equation[2]:

$$s = \frac{a_n - a_0}{a_0} \times 100\% \quad (1)$$

Where a_0 is the lattice parameter of PtBi NFBs (that is, 0.3737; ICSD PDF # 58845), and a_n is the lattice parameter of Cu-PtBi NFBs. As determined from the PXRD data, the lattice parameter for Cu-PtBi NFBs is 0.3691, suggesting a compressive strain of 1.23%. Furthermore, EXAFS analysis reveals that the compressive strain of Cu-PtBi NFBs is 1.06%. Therefore, we estimate the compressive strain of Cu-PtBi NFBs is 1.15% (average value).

Electrochemical measurements

Before the electrochemical measurements, the obtained catalysts were loaded on commercial carbon black (Vulcan XC-72R) and the loading amounts of Pt for Cu-PtBi NFBs/C, PtBi NFBs/C, and PtCu NFBs/C were determined to be 7.1, 10.1, and 10.5 wt.%, respectively, according to the results of ICP-AES. Then 2 mg of carbon-supported catalysts were added into a mixture containing 1000 μL of isopropanol, 960 μL of ultrapure water, and 40 μL of Nafion solution, followed by ultrasonication for 1 h to obtain a well-suspended catalyst ink. Finally, 10 μL of ink was dropped onto a glassy carbon electrode (GCE) with a diameter of 4 mm for the following measurements.

All the electrochemical measurements were carried out in a typical three-electrode cell using a CHI760e electrochemical analyzer (CH Instruments, Inc., Shanghai). The catalyst-coated GCE (area: 0.1256 cm^2) was used as the working electrode. A saturated calomel electrode (SCE) and Pt foil were used as the reference electrode and the conference electrode, respectively. The cyclic voltammetry (CV) curves were performed in Ar-saturated 1.0 M KOH solution between 0.05-1.1 V *vs*. RHE at a scan rate of 50 mV s^{-1}. For methanol oxidation reaction (MOR)/ethanol oxidation reaction (EOR), the CV curves were measured in Ar-saturated 1.0 M KOH with 0.5 M methanol/ethanol solution. For stability tests,

chronoamperometric (CA) tests were carried out for 5000 s at the work potential of 0.79 V *vs*. RHE for MOR and 0.77 V *vs*. RHE for EOR. For CO stripping measurements, CO gas was bubbled into 1.0 M KOH while holding the working electrode potential at 0.1 V *vs*. RHE for 15 min. After that, two CV curves were recorded between 0.05-1.2 V *vs*. RHE in Ar-saturated 1.0 M KOH solution at a scan rate of 20 mV s^{-1}.

The electrochemical active surface areas (ECSAs) of the Pt-based catalysts were determined from charges associated with underpotentially deposited Cu (Cu_{upd}). Generally, the Cu stripping tests were carried out in Ar-saturated 2 mM $CuSO_4$ with 0.05 M H_2SO_4 solution. Firstly, the potential was set at 0.3 V *vs*. RHE and kept for 100 s to form a full monolayer adsorbed Cu. Then the CV curves were acquired from 0.3 to 1.2 V *vs*. RHE at a scan rate of 20 mV s^{-1}. The ECSAs were calculated according to the following equation[2]:

$$\mathrm{ECSA} = \frac{Q}{[M]\theta} \tag{2}$$

Where Q (mC) is the charge for the Cu_{upd}, θ (0.470 mC cm^{-2}) is the charge density, and $[M]$ (mg) is the mass of Pt loaded on the electrode.

Density functional theory (DFT) calculations.

DFT calculations were conducted *via* Vienna Ab initio Simulation Package[3]. The exchange-correlation energy was described by using the revised Perdew-Burke-Ernzerhof exchange-correlation density functional within the generalized gradient approximation[4, 5]. A 400 eV of plane-wave kinetic energy cut-off was chosen. We created 3 × 3 × 1 supercells with four atomic layers to simulate Pt(111) and PtCu(111) surface. The PtBi(100) and PtSnBi(100) surfaces were built by creating 2 × 2 × 1 supercells. The atomic positions were fully relaxed until a maximum energy difference and residual force on atoms, respectively, converged to 10^{-6} eV and 0.03 eV $Å^{-1}$ eV, and a 15 Å thick vacuum layer was used to avoid the interaction between top and bottom surfaces. The free energies of the electrochemical steps of the reaction were calculated based on the computational hydrogen electrode (CHE) model. The free energies of species were calculated as follows:

$$G = E_{DFT} + E_{ZPE} - T\Delta S \tag{3}$$

where E_{DFT} was obtained from DFT energy, E_{ZPE} and $T\Delta S$ of adsorbed species were calculated by vibration analysis. The thermodynamic corrections for gas molecules were achieved from the standard

database.

Supplementary Figures

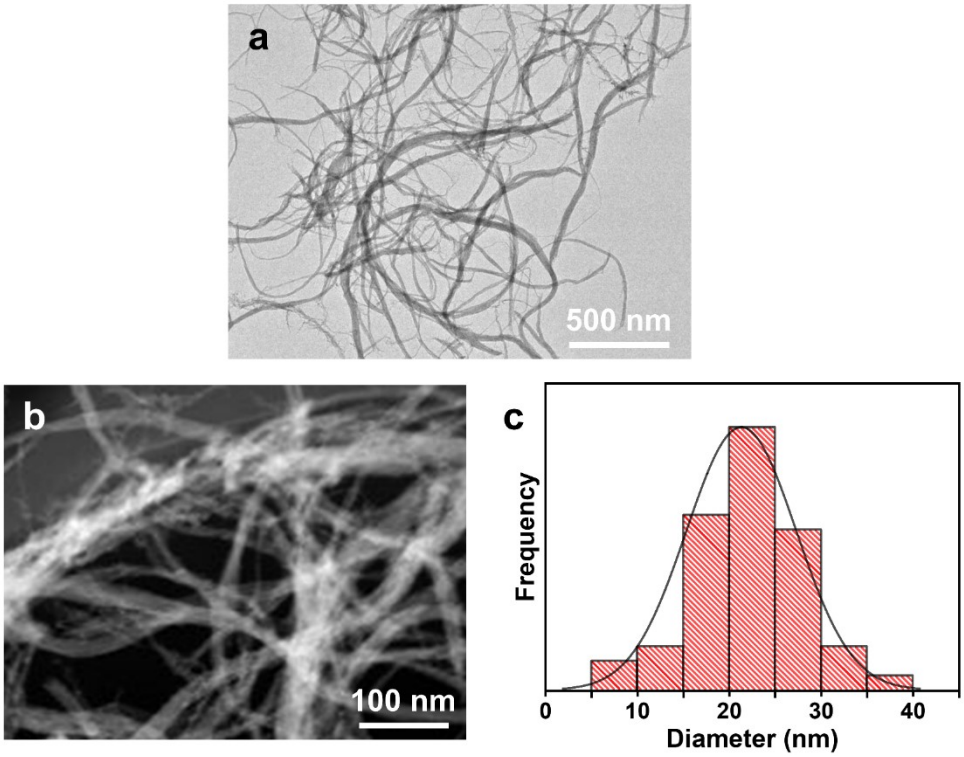

Fig. S1. (a) TEM image, (b) HAADF-STEM image, and (c) histogram of the diameter of Cu-PtBi NFBs.

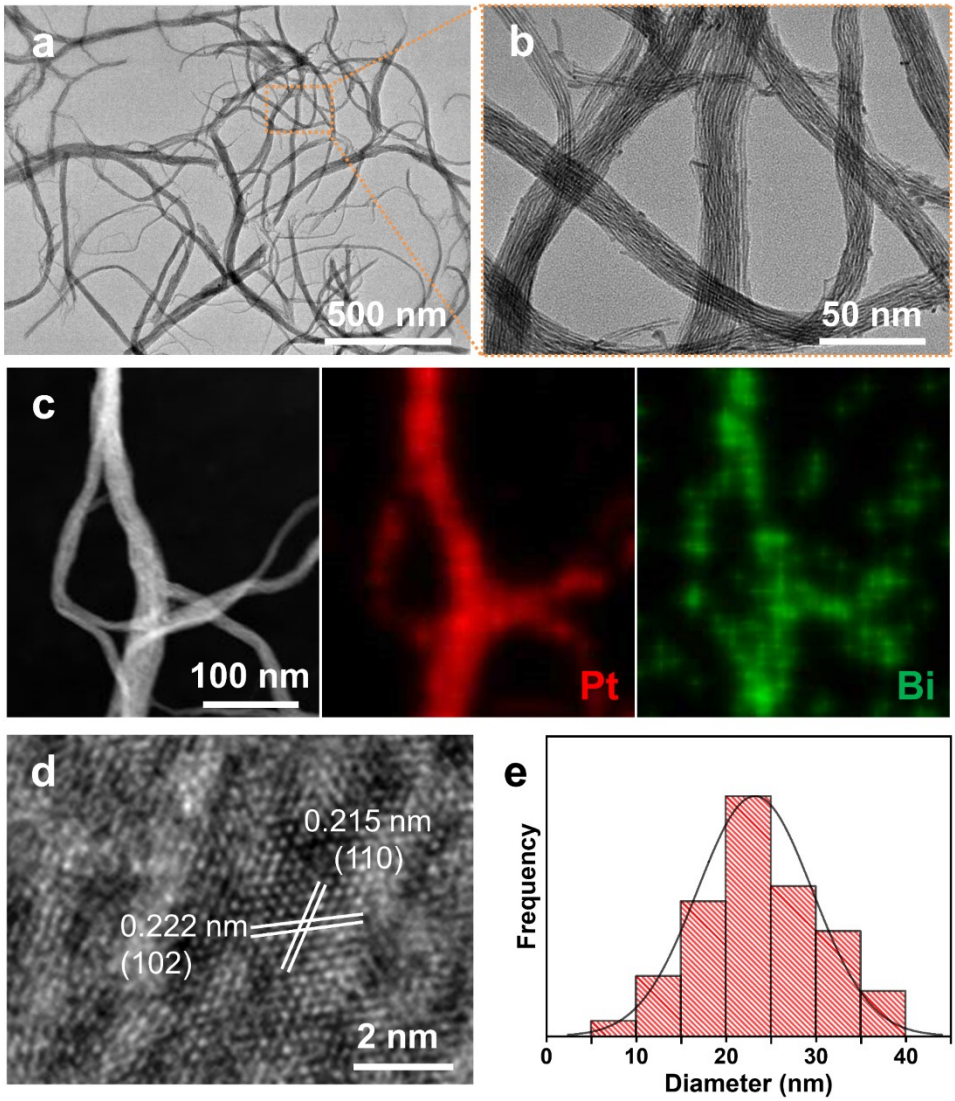

Fig. S2. (a,b) TEM images, (c) EDS elemental mapping, (d) HRTEM image, and (e) histogram of the diameter of PtBi NFBs.

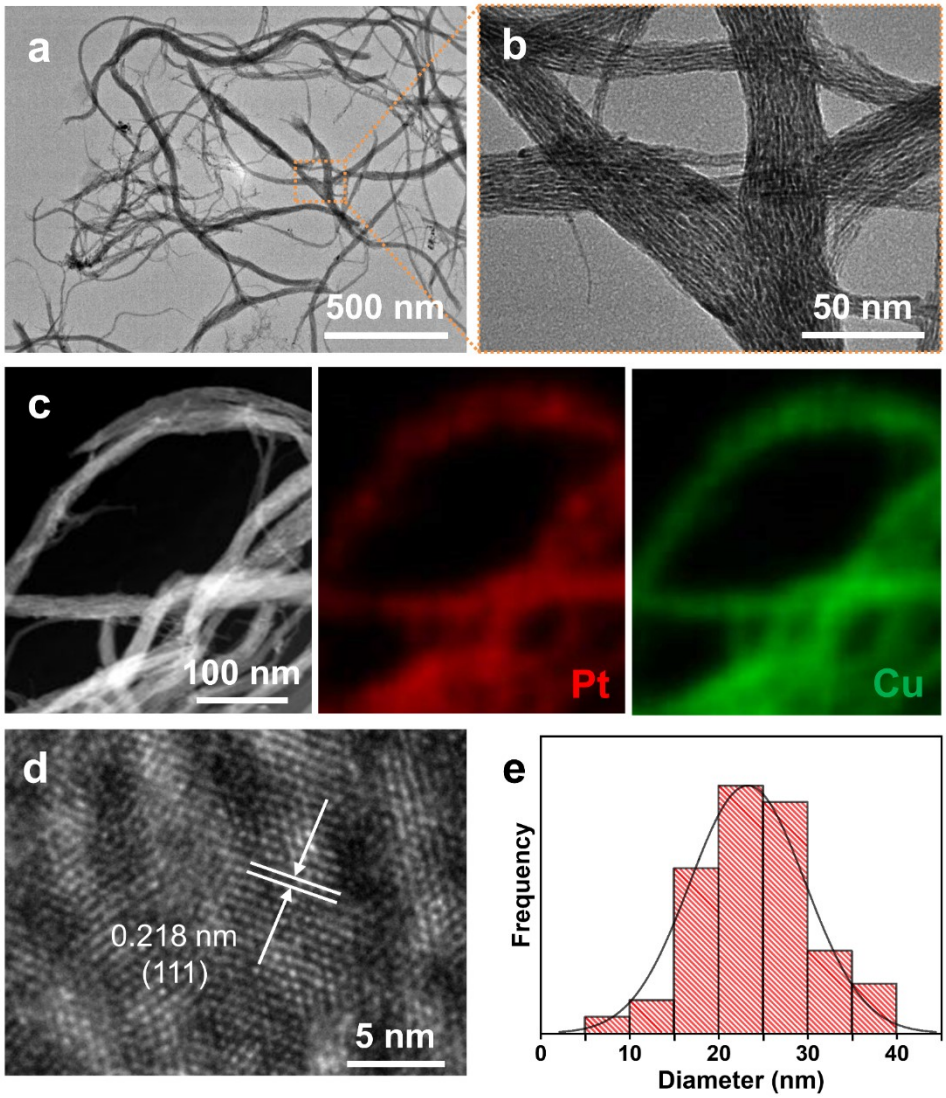

Fig. S3. (a,b) TEM images, (c) EDS elemental mapping, (d) HRTEM image, and (e) histogram of the diameter of PtCu NFBs.

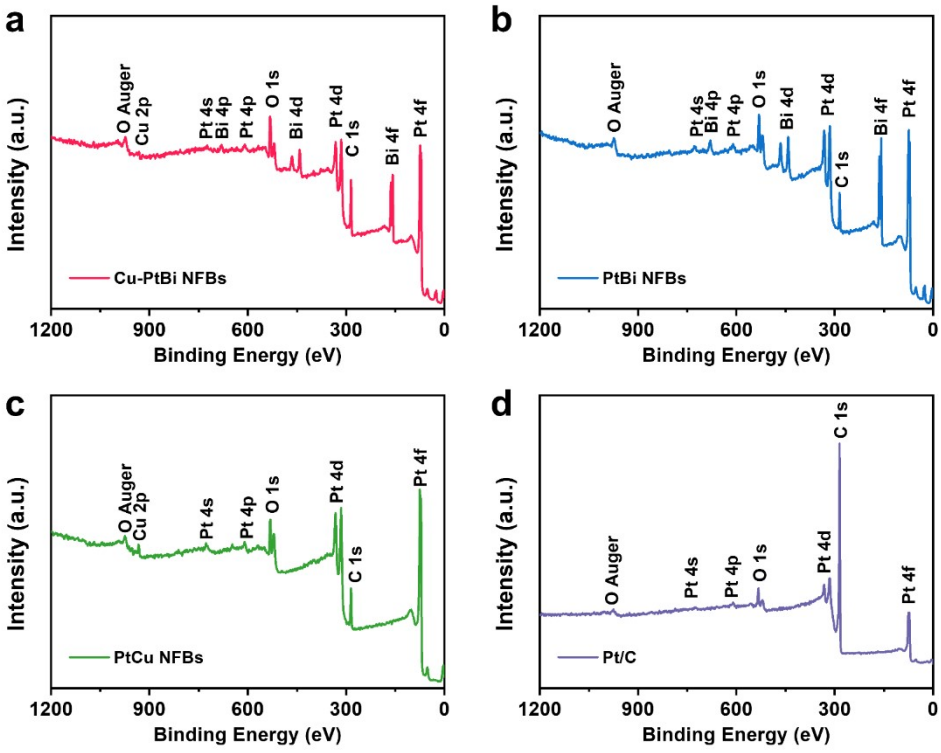

Fig. S4. XPS survey spectra of (a) Cu-PtBi NFBs, (b) PtBi NFBs, (c) PtCu NFBs, and (d) commercial Pt/C.

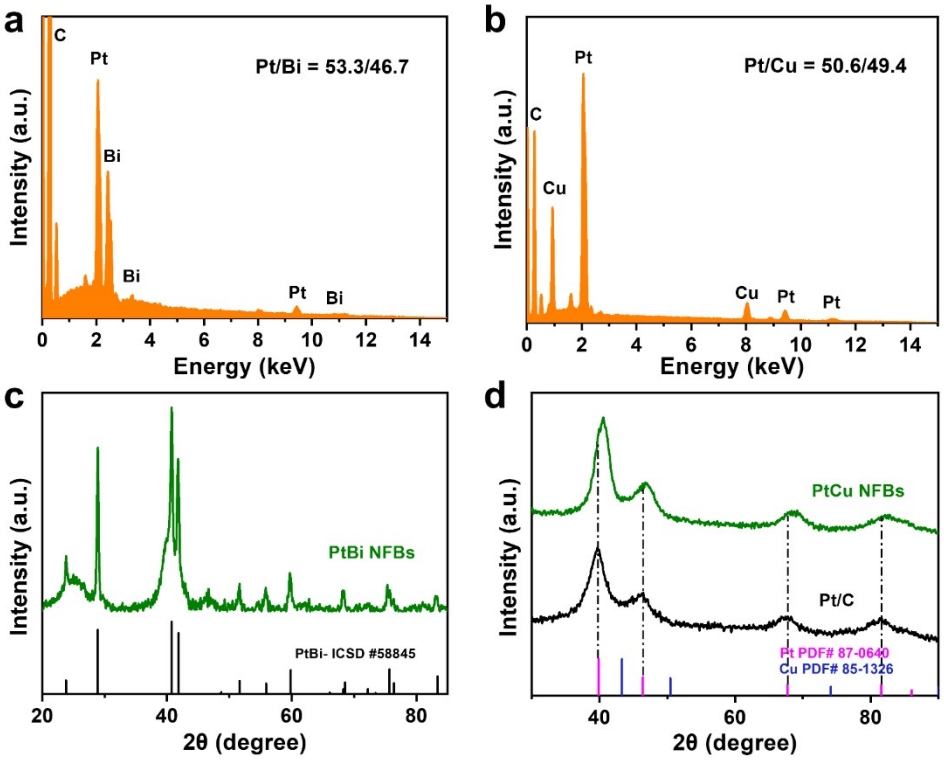

Fig. S5. (a) EDS and (c) PXRD pattern of PtBi NFBs, (b) EDS pattern of PtCu NFBs, and (d) PXRD patterns of PtCu NFBs and commercial Pt/C.

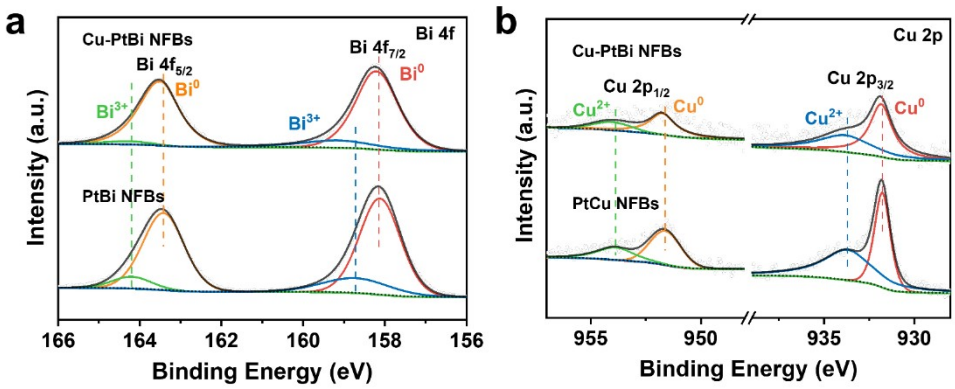

Fig. S6. (a) Bi 4f XPS spectra recorded from Cu-PtBi NFBs and PtBi NFBs. (b) Cu 2p XPS spectra recorded from Cu-PtBi NFBs and PtCu NFBs.

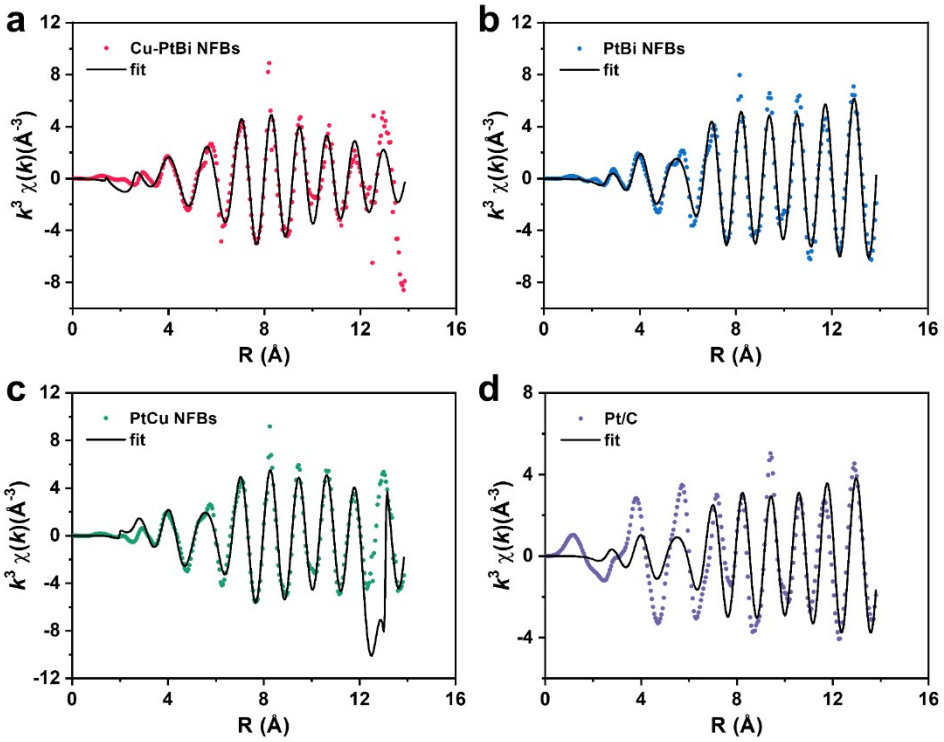

Fig. S7. Pt L_3-edge EXAFS (points) and the curve fit (line) in k^3-weighted k-space for (a) Cu-PtBi NFBs, (b) PtBi NFBs, (c) PtCu NFBs, and (d) commercial Pt/C.

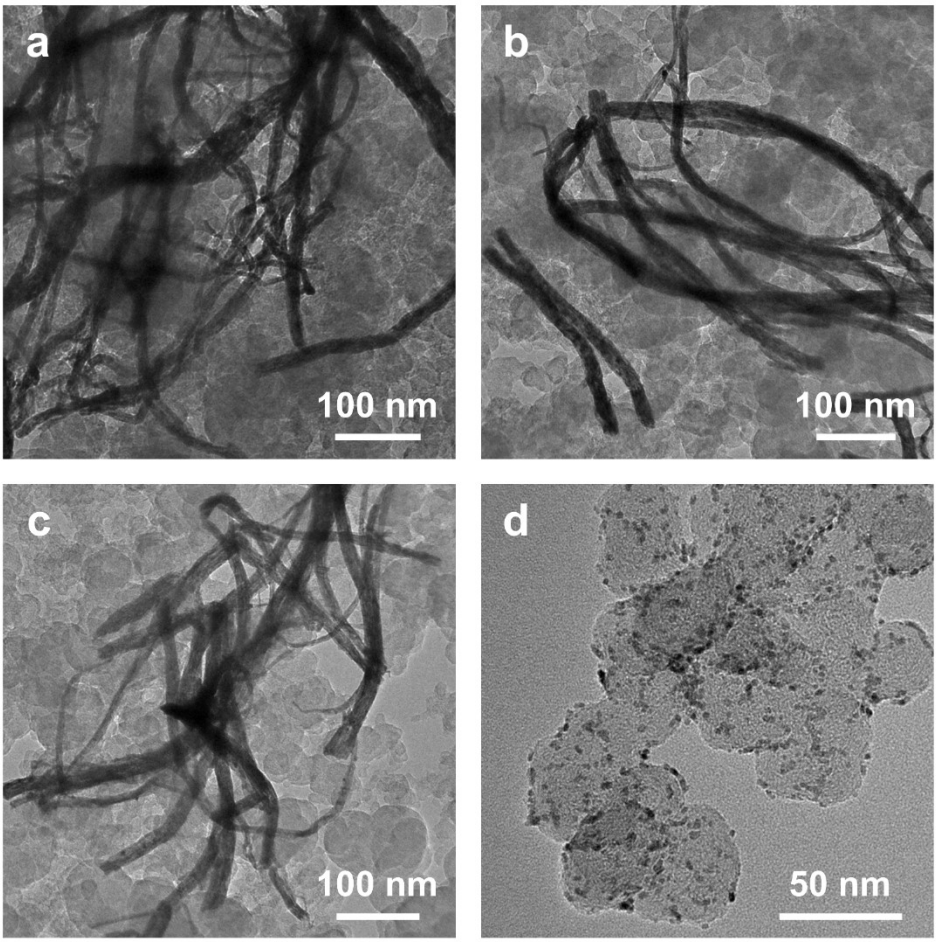

Fig. S8. TEM images of (a) Cu-PtBi NFBs/C, (b) PtBi NFBs/C, (c) PtCu NFBs/C, and (d) commercial Pt/C.

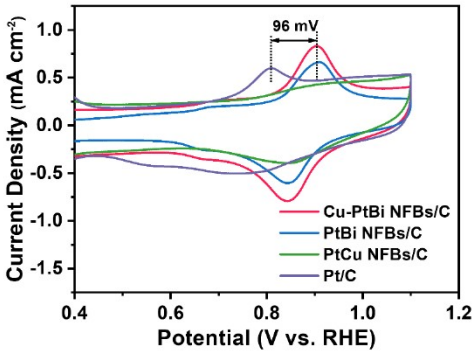

Fig. S9. Enlarged CV curves (the Pt-OH regions) of **Fig. 3a** for Pt-based catalysts.

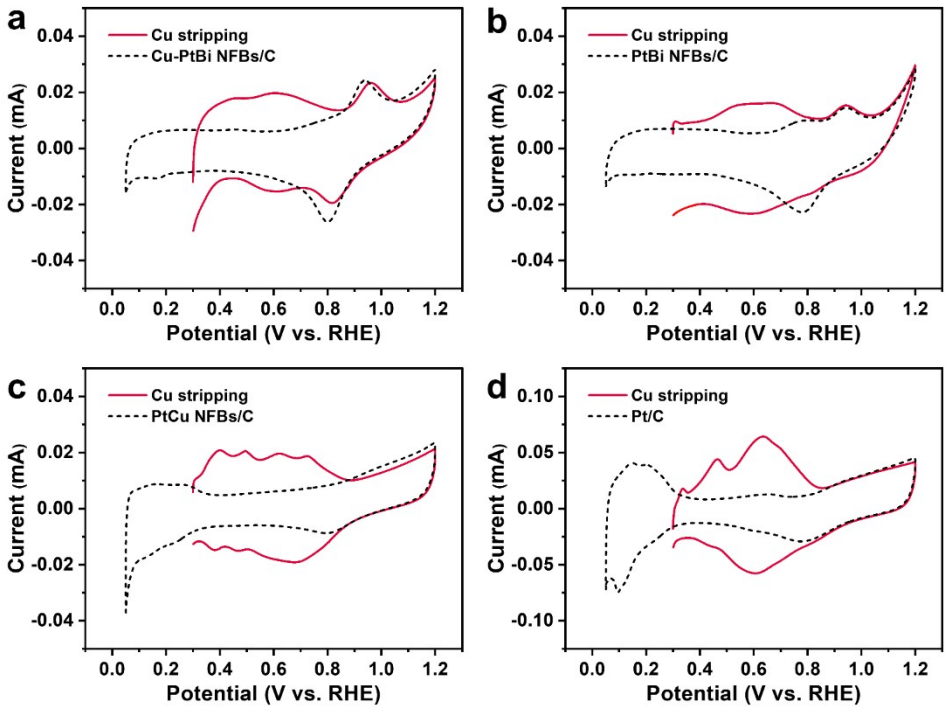

Fig. S10. Cu stripping voltammograms of (a) Cu-PtBi NFBs/C, (b) PtBi NFBs/C, (c) PtCu NFBs/C, and (d) commercial Pt/C recorded in 0.05 M H_2SO_4 with 2 mM $CuSO_4$ solution at a scan rate of 20 mV s^{-1}.

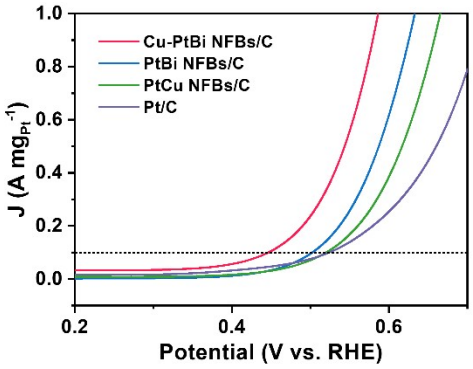

Fig. S11. Enlarged CV curves (onset potentials) of **Fig. 3b** for Pt-based catalysts.

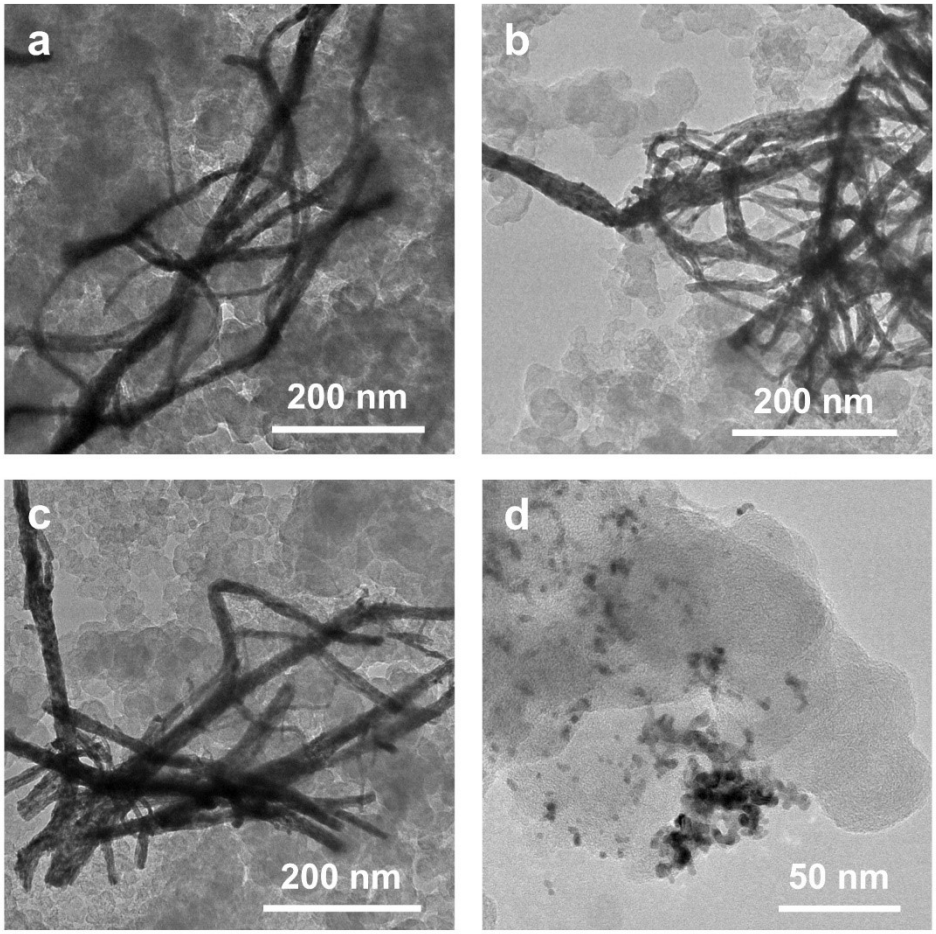

Fig. S12. TEM images of (a) Cu-PtBi NFBs/C, (b) PtBi NFBs/C, (c) PtCu NFBs/C, and (d) commercial Pt/C after the durability tests.

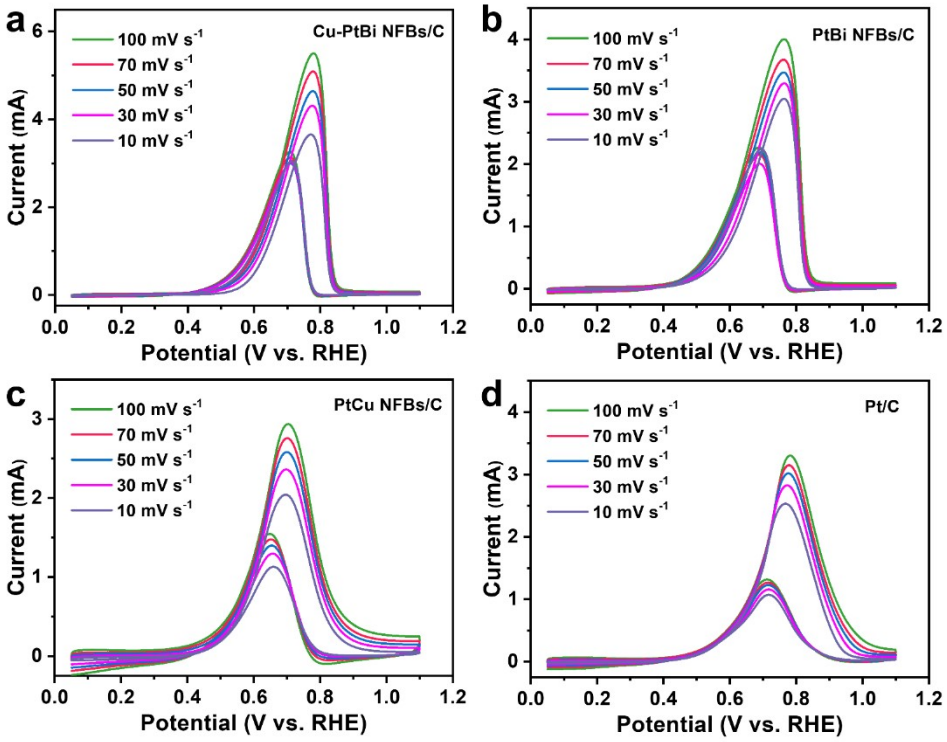

Fig. S13. CV curves of (a) Cu-PtBi NFBs/C, (b) PtBi NFBs/C, (c) PtCu NFBs/C, and (d) commercial Pt/C in 1.0 M KOH solution with 0.5 M CH_3OH at different scan rates.

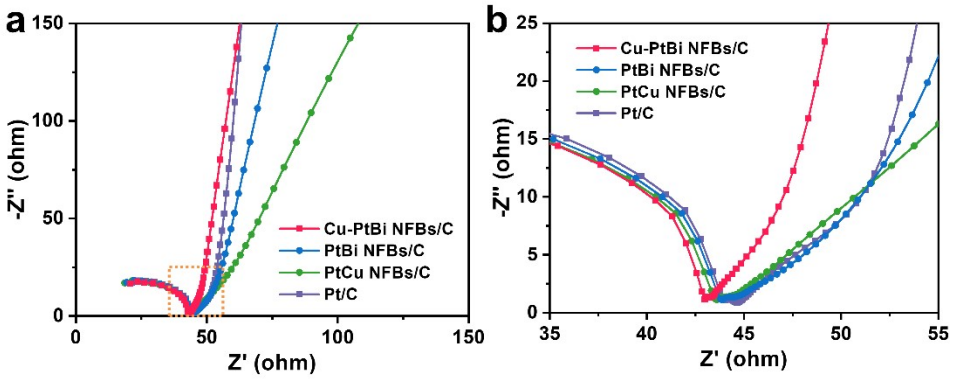

Fig. S14. (a) Nyquist plots of these catalysts and (b) is the enlarged area in (a).

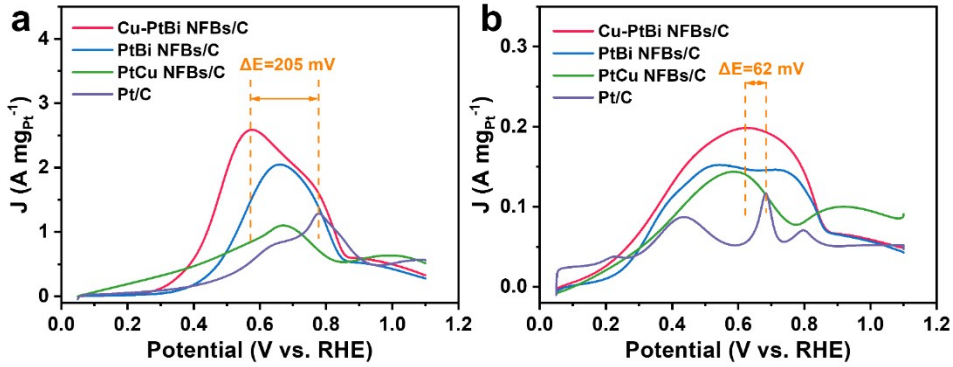

Fig. S15. CV curves of different catalysts in 1.0 M KOH solution with (a) 0.1 M HCHO and (b) 0.1 M HCOOH.

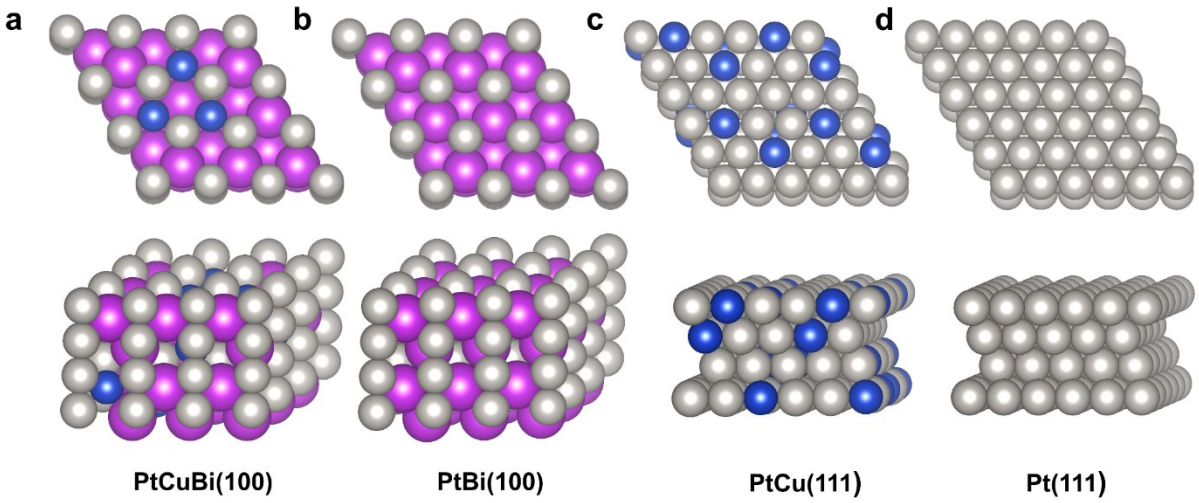

Fig. S16. Top view (up) and side view (down) for the Pt-based models: (a) PtCuBi(100), (b) PtBi(100), (c) PtCu(111), and (d) Pt(111). Color code: gray, Pt; dark blue, Cu; purple, Bi.

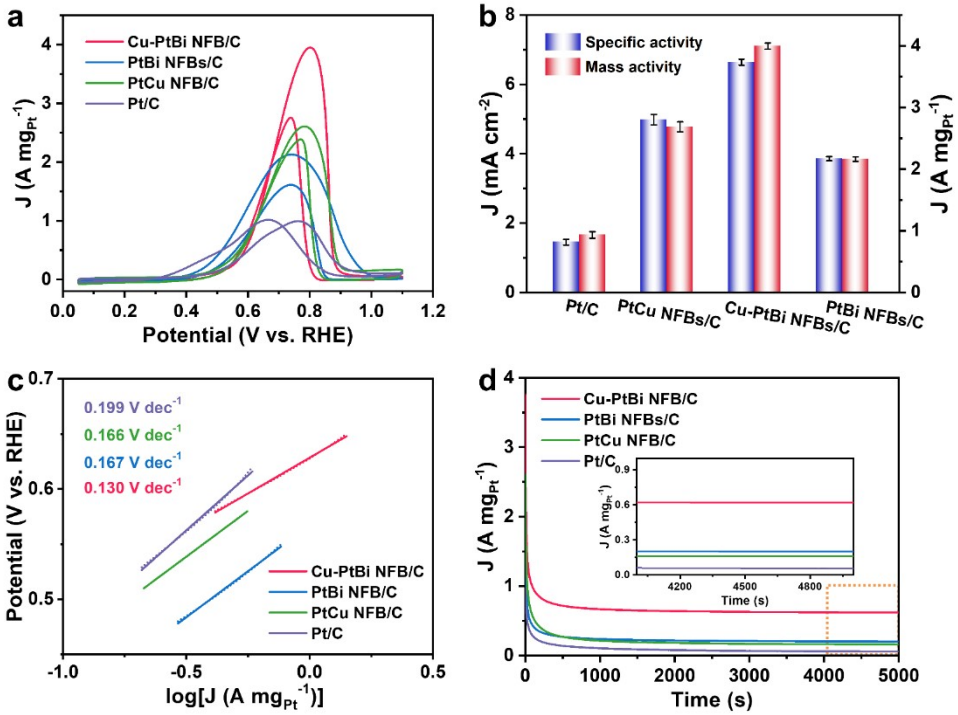

Fig. S17. Electrocatalysis performance of various Pt-based catalysts towards EOR. (a) Pt mass-normalized CV curves in 1.0 M KOH solution with 0.5 M C_2H_5OH, (b) specific and mass activities, (c) the Tafel plots, and (d) CA measurements at 0.77 V *vs*. RHE (inset: enlarged i-t curves from 4000 to 5000 s).

Table S1. The atomic percentage of Pt, Bi, and Cu in the Cu-PtBi NFBs, PtBi NFBs, and PtCu NFBs obtained from ICP-AES and SEM-EDS.

Catalysts	Atomic ratios of Pt/Bi/Cu (%)	
	ICP-AES result	**SEM-EDS result**
Cu-PtBi NFBs	44.9/26.7/28.4	44.0/26.1/29.9
PtBi NFBs	52.2/47.8/-	53.3/46.7/-
PtCu NFBs	49.8/-/50.2	50.6/-/49.4

Table S2. Summary of Pt L_3-edge EXAFS fitting results for Cu-PtBi NFBs, PtBi NFBs, PtCu NFBs, and commercial Pt/C.

Catalysts	Pt-Pt path R (Å)	CN	σ^2 (Å^2)	ΔE_0 (eV)
Cu-PtBi NFBs	2.81±0.03	4.5±0.9	0.011±0.001	7.4±2.1
PtBi NFBs	2.84±0.01	6.7±0.6	0.005±0.004	7.9±1.1
PtCu NFBs	2.73±0.04	8.4±1.0	0.007±0.001	6.6±0.9
Pt/C	2.74±0.04	5.1±0.9	0.006±0.001	5.7±1.2

R, distance between absorber and backscatter atoms; CN, coordination number; σ^2, Debye-Waller factor; ΔE_0, inner potential correction to account for the difference in the inner potential between the catalysts and the reference.

Table S3. Summary of reported catalytic performance of various Pt-based MOR catalysts in alkaline electrolyte.

Catalysts	Electrolyte	Mass activity (A/mg_{Pt})	Specific activity (mA/cm^2)	Reference
Cu-PtBi NFBs/C	1.0 M KOH, 0.5 M CH_3OH	6.79	11.26	This work
PtBi NFBs/C	1.0 M KOH, 0.5 M CH_3OH	3.12	5.56	This work
PtCu NFBs/C	1.0 M KOH, 0.5 M CH_3OH	2.49	4.63	This work
Pt/C	1.0 M KOH, 0.5 M CH_3OH	1.49	2.30	This work
Au@Pt_1–Pd_1 H-Ss	1.0 M KOH, 1.0 M CH_3OH	4.38	5.04	6
PtCo NF	1.0 M KOH, 1.0 M CH_3OH	4.28	8.56	7
PdPtCu MHS@N-G	1.0 M KOH, 1.0 M CH_3OH	3.01	-	8
Pt/$Ni(OH)_2$/NG	1.0 M KOH, 1.0 M CH_3OH	2.99	4.82	9
Pt-$Ce(CO_3)OH$/rGO	1.0 M KOH, 1.0 M CH_3OH	1.48	2.45	10
$PtCu_3$ nanosheets	0.5 M KOH, 1.0 M CH_3OH	3.05	9.96	11
Pt_1Ni_1/C	1.0 M KOH, 1.0 M CH_3OH	1.75	4.9	12
PtZn/MWNT-E	0.1 M KOH, 0.5 M CH_3OH	0.55	1.14	13
Porous Pt NTs	1.0 M KOH, 1.0 M CH_3OH	2.33	~4.90	14
Pt/$Ni(OH)_2$/rGO	1.0 M KOH, 1.0 M CH_3OH	1.24	1.93	15

Table S4. Calculated reaction barriers (ΔG) of the MOR elementary steps over PtCuBi(100).

Elementary steps	**ΔG (eV)**
$*CH_3OH \rightarrow *CH_2OH + *H$	0.29
$*CH_2OH \rightarrow *CHOH + *H$	-0.17
$*CHOH \rightarrow *COH + *H$	0.39
$*COH \rightarrow *CO + *H$	-0.81
$*CO + *OH \rightarrow *COOH$	0.57
$*COOH \rightarrow *COO + *H$	-0.73
$*COO \rightarrow CO_2$	0.04

Table S5. Calculated reaction barriers (ΔG) of the MOR elementary steps over Pt(111).

Elementary steps	**ΔG (eV)**
$*CH_3OH \rightarrow *CH_2OH + *H$	0.35
$*CH_2OH \rightarrow *CHOH + *H$	-0.17
$*CHOH \rightarrow *COH + *H$	0.44
$*COH \rightarrow *CO + *H$	-0.98
$*CO + *OH \rightarrow *COOH$	0.76
$*COOH \rightarrow *COO + *H$	-0.92
$*COO \rightarrow CO_2$	0.04

Table S6. Summary of reported catalytic performance of various Pt-based EOR catalysts in alkaline electrolyte.

Catalysts	Electrolyte	Mass activity (A/mg_{Pt})	Specific activity (mA/cm^2)	Reference
Cu-PtBi NFBs/C	1.0 M KOH, 0.5 M C_2H_5OH	4.00	6.64	This work
PtBi NFBs/C	1.0 M KOH, 0.5 M C_2H_5OH	2.16	3.86	This work
PtCu NFBs/C	1.0 M KOH, 0.5 M C_2H_5OH	2.69	4.98	This work
Pt/C	1.0 M KOH, 0.5 M C_2H_5OH	0.93	1.45	This work
Au@Pt_1–Pd_1 H-Ss	1.0 M KOH, 1.0 M C_2H_5OH	3.18	3.66	6
Pt/α-PtO_x/WO_3	0.1 M NaOH, 0.5 M C_2H_5OH	2.76	1.56	16
PtPdNiCu TNTPs	1.0 M KOH, 1.0 M C_2H_5OH	1.019	-	17
$Pd_{43}Ag_{21}Pt_{36}$	1.0 M KOH, 1.0 M C_2H_5OH	3.33	~5.20	18
Pt69Rh8Fe23-PNS@MXene	1.0 M KOH, 1.0 M C_2H_5OH	3.41	-	19
PtCuRh NWs	1.0 M KOH, 1.0 M C_2H_5OH	2.01	-	20
PtRh@SnO_2 NW/C	1.0 M NaOH, 1.0 M C_2H_5OH	3.16	5.63	21
PtSn nanosheets	0.2 M KOH, 0.2 M C_2H_5OH	0.67	1.02	22
Pt_1Ru_1/C	0.1 M NaOH, 0.1 M C_2H_5OH	3.73	-	23
Pd-Pt-Ag nanosheets	1.0 M KOH, 0.5 M C_2H_5OH	~1.32	2.41	24

Supplementary References

1. B. Ravel and M. Newville, *J. Synchrotron Radiat.*, 2005, **12**, 537-541.
2. M. Luo, Z. Zhao, Y. Zhang, Y. Sun, Y. Xing, F. Lv, Y. Yang, X. Zhang, S. Hwang, Y. Qin, J.-Y. Ma, F. Lin, D. Su, G. Lu and S. Guo, *Nature*, 2019, **574**, 81-85.
3. J. P. Perdew, K. Burke and M. Ernzerhof, *Phys. Rev. Lett.*, 1997, **78**, 1396-1396.
4. P. E. Blochl, *Phys. Rev. B*, 1994, **50**, 17953-17979.
5. J. P. Perdew, K. Burke and M. Ernzerhof, *Phys. Rev. Lett.*, 1996, **77**, 3865-3868.
6. W. Liang, Y. Wang, L. Zhao, W. Guo, D. Li, W. Qin, H. Wu, Y. Sun and L. Jiang, *Adv. Mater.*, 2021, 2100713.
7. S. Chen, M. Li, M. Gao, J. Jin, M. A. van Spronsen, M. B. Salmeron and P. Yang, *Nano Lett.*, 2020, **20**, 1974-1979.
8. L. Sun, H. Lv, D. Xu and B. Liu, *J. Mater. Chem. A*, 2020, **8**, 15706-15714.
9. K. Zhang, H. Wang, J. Qiu, J. Wu, H. Wang, J. Shao, Y. Deng and L. Yan, *Chem. Eng. J.*, 2020, 127786.
10. G. Chen, Z. Dai, L. Sun, L. Zhang, S. Liu, H. Bao, J. Bi, S. Yang and F. Ma, *J. Mater. Chem. A*, 2019, **7**, 6562-6571.
11. F. Wu, W. Niu, J. Lai, W. Zhang, R. Luque and G. Xu, *Small*, 2019, **15**, 1804407.
12. J. T. L. Gamler, H. M. Ashberry, S. E. Skrabalak and K. M. Koczkur, *Adv. Mater.*, 2018, **30**, 1801563.
13. Z. Qi, C. Xiao, C. Liu, T. W. Goh, L. Zhou, R. Maligal-Ganesh, Y. Pei, X. Li, L. A. Curtiss and W. Huang, *J. Am. Chem. Soc.*, 2017, **139**, 4762-4768.
14. Y. Lou, C. Li, X. Gao, T. Bai, C. Chen, H. Huang, C. Liang, Z. Shi and S. Feng, *ACS ACS Appl. Mater. Interfaces*, 2016, **8**, 16147-16153.
15. W. Huang, H. Wang, J. Zhou, J. Wang, P. N. Duchesne, D. Muir, P. Zhang, N. Han, F. Zhao, M. Zeng, J. Zhong, C. Jin, Y. Li, S.-T. Lee and H. Dai, *Nat. Commun.*, 2015, **6**, 10035.
16. L. Xiao, G. Li, Z. Yang, K. Chen, R. Zhou, H. Liao, Q. Xu and J. Xu, *Adv. Funct. Mater.*, 2021, **n/a**, 2100982.
17. Y.-G. Feng, H.-J. Niu, L.-P. Mei, J.-J. Feng, K.-M. Fang and A.-J. Wang, *J. Colloid Interface Sci.*, 2020, **575**, 425-432.
18. W. Lu, X. Xia, X. Wei, M. Li, M. Zeng, J. Guo and S. Cheng, *ACS Appl. Mater. Interfaces*, 2020, **12**, 21569-21578.
19. P. Wang, H. Cui and C. Wang, *Nano Energy*, 2019, **66**, 104196.
20. C. Chen, H. Xu, H. Shang, L. Jin, T. Song, C. Wang, F. Gao, Y. Zhang and Y. Du, *Nanoscale*, 2019, **11**, 20090-20095.
21. X. Fan, M. Tang, X. Wu, S. Luo, W. Chen, X. Song and Z. Quan, *J. Mater. Chem. A*, 2019, **7**, 27377-27382.
22. J.-Y. Chen, S.-C. Lim, C.-H. Kuo and H.-Y. Tuan, *J. Colloid Interface Sci.*, 2019, **545**, 54-62.
23. Z. Gu, S. Li, Z. Xiong, H. Xu, F. Gao and Y. Du, *J. Colloid Interface Sci.*, 2018, **521**, 111-118.
24. J. W. Hong, Y. Kim, D. H. Wi, S. Lee, S.-U. Lee, Y. W. Lee, S.-I. Choi and S. W. Han, *Angew. Chem. Int. Ed.*, 2016, **55**, 2753-2758.